Available online at www.sciencedirect.com
SCIENCE DIRECT
Solid State Ionics 177 (2006) 457 – 470
SOLID STATE IONICS
www.elsevier.com/locate/ssi

Defect interactions in $La_{0.3}Sr_{0.7}Fe(M')O_{3-\delta}$ (M' = Al, Ga) perovskites: Atomistic simulations and analysis of $p(O_2)$-T-δ diagrams

E.N. Naumovich [a,b], M.V. Patrakeev [a,c], V.V. Kharton [a,b,*], M.S. Islam [d], A.A. Yaremchenko [a], J.R. Frade [a], F.M.B. Marques [a]

[a] Department of Ceramics and Glass Engineering, CICECO, University of Aveiro, 3810-193 Aveiro, Portugal
[b] Institute of Physicochemical Problems, Belarus State University, 14 Leningradskaya Str., 220050 Minsk, Belarus
[c] Institute of Solid State Chemistry, Ural Branch of RAS, 91 Pervomaiskaya Str., 620219 Ekaterinburg, Russia
[d] Chemistry Division, University of Surrey, Guildford GU2 4BS, United Kingdom

Received 12 November 2004; received in revised form 15 October 2005; accepted 28 November 2005

Abstract

Atomistic modelling showed that a key factor affecting the $p(O_2)$ dependencies of point defect chemical potentials in perovskite-type $La_{0.3}Sr_{0.7}Fe_{1-x}M'_xO_{3-\delta}$ (M' = Ga, Al; $x = 0-0.4$) under oxidizing conditions, relates to the coulombic repulsion between oxygen vacancies and/or electron holes. The configurations of A- and B-site cations with stable oxidation states have no essential influence on energetics of the mobile charge carriers, whereas the electrons formed due to iron disproportionation are expected to form defect pair clusters with oxygen vacancies. These results were used to develop thermodynamic models, adequately describing the $p(O_2)$-T-δ diagrams of $La_{0.3}Sr_{0.7}Fe(M')O_{3-\delta}$ determined by the coulometric titration technique at 923–1223 K in the oxygen partial pressure range from 1×10^{-5} to 0.5 atm. The thermodynamic functions governing the oxygen intercalation process were found independent of the defect concentration. Doping with aluminum and gallium leads to increasing oxygen deficiency and induces substantial changes in the behavior of iron cations, increasing the tendencies to disproportionation and hole localization. Despite similar oxygen nonstoichiometry in the Al- and Ga-substituted ferrites at a given dopant content, the latter tendency is more pronounced in the case of aluminum-containing perovskites.

Keywords: Oxygen nonstoichiometry; Defect interaction; Atomistic simulations; Ferrite; Perovskite

1. Introduction

Oxide phases with mixed oxygen-ionic and electronic conductivity are of great interest for high-temperature electrochemical applications, such as electrodes of solid oxide fuel cells (SOFCs), dense ceramic membranes for oxygen separation and partial oxidation of light hydrocarbons, and sensors [1–7]. In particular, the use of mixed-conducting membranes for conversion of methane to CO and H_2, the most important feedstock for commercial Fischer–Tropsch and methanol synthesis, is expected to provide substantial economic benefits [1,3]. The membrane materials should satisfy numerous requirements including high oxygen permeability, stability in a wide range of oxygen partial pressure and temperature, and suitable thermomechanical properties. One promising group of mixed conductors relates to the perovskite-like solid solutions based on strontium–lanthanum ferrites, (Sr, La)$FeO_{3-\delta}$, which possess an attractive level of oxygen transport when the concentration of ionic charge carriers, oxygen vacancies, is high enough [1–12]. Most ferrite ceramics exhibit, however, insufficient thermodynamic and dimensional stability under large oxygen chemical potential gradients [3,6,7]. In addition, ordering in the oxygen sublattice at reduced $p(O_2)$ results in deterioration of ionic conduction and, hence, oxygen permeation through membranes [8–10]. To some extent, the stability can be improved

* Corresponding author. Present address: Department of Ceramics and Glass Engineering, CICECO, University of Aveiro, 3810-193 Aveiro, Portugal. Tel.: +351 234 370263; fax: +351 234 425300.
E-mail address: kharton@cv.ua.pt (V.V. Kharton).

0167-2738/$ - see front matter © 2005 Elsevier B.V. All rights reserved.
doi:10.1016/j.ssi.2005.11.022

by partial substitution of iron for metal cations having a more stable oxidation state under the membrane operation conditions, such as Cr [3,5,6], Ti [6,10], Ga [7,11] or Al [12], in order to suppress oxygen stoichiometry variations and/or to preserve perovskite-related structure under the membrane operation conditions. Certainly, these substitutions have strong influence on the transport and physicochemical properties of the solid solutions. Development of new mixed conductors based on (Sr, La)$FeO_{3-\delta}$ requires, therefore, systematic studies of the oxygen deficiency and defect interaction or association processes, which all affect the material stability and ionic conduction, as functions of the oxygen partial pressure, temperature and cation composition.

In a first approximation, the defect chemistry of perovskites, where the oxygen nonstoichiometry is low and the electronic charge carriers are localized, can be described using the ideal solution model and its derivatives [12–17]. These postulate, in particular, random distribution of point defects and/or simplest defect clusters in the structure, zero interaction between different sublattices and negligible coulombic attraction/repulsion between the defects, except for the crystal electroneutrality condition. However, for highly nonstoichiometric oxide systems such as Fe-, Co- and Cu-containing compounds, such assumptions are not valid any more [10,17–19], though can still be used to predict general trends or to describe selected relationships between the defect concentrations and oxygen partial pressure in a narrow $p(O_2)$ range [2,8,12,13,20].

This work presents a thermodynamic model, based on the atomistic computer simulations and verified using experimental $p(O_2)$-T-δ diagrams, for the description of defect formation and interaction processes in perovskite-type solid solutions $La_{0.3}Sr_{0.7}Fe(M')O_{3-\delta}$ (M' = Al, Ga) under oxidizing conditions. The characterization results of the title materials, including crystal structure, transport properties, thermal and chemical induced expansion, are found in Refs. [11,12,18,21,22]. The $p(O_2)$-T-δ diagrams of $La_{0.3}Sr_{0.7}Fe_{1-x}Ga_xO_{3-\delta}$ and their preliminary analysis were also published elsewhere [18]. If compared to Ga doping, the substitution of iron with aluminum may be preferable for practical applications due to well-known disadvantages of Ga-containing ceramics, namely the high costs, volatilization of gallium oxide at elevated temperatures and/or in reducing atmospheres, and possible interaction with catalysts such as Pt or Ni [23]. The atomistic simulation work uses well-established methods [24,25], applied successfully in previous computational studies of defects and ion transport in perovskite phases such as $LaGaO_3$ [26–28].

2. Basic relationships

2.1. Gas–solid equilibrium

Under oxidizing conditions studied in this work, $p(O_2) = 1\times10^{-5} - 0.5$ atm and $T = 923 - 1223$ K, all $La_{0.3}Sr_{0.7}Fe_{1-x}M'_xO_{3-\delta}$ (M' = Al, Ga; $x = 0 - 0.4$) possess a cubic perovskite structure and predominant p-type electronic conductivity via a hopping mechanism [11,12,18,21]. In the subsequent discussion, the standard state of these perovskites was selected as $A^{III}B^{III}O_3$; the oxygen vacancies, Sr^{2+} cations and electron holes are hence considered as positively charged defects. The process of oxygen incorporation in the perovskite lattice may thus be formulated as

$$O_2(gas) + 2V_o^{\bullet\bullet} \rightleftarrows 4h_B^{\bullet} + 2O_o^{\times} \quad (1)$$

where the Kroger–Vink notation is used, and the holes are localized on the variable-valence iron cations, forming Fe^{4+} (or $Fe_B^{\bullet}$). In equilibrium, the chemical potentials (μ) of all species participating in the oxygen exchange reaction should be related as

$$\sum_z m_z \cdot \mu(z) = 0 \quad (2)$$

with m_z being the stoichiometric coefficient of z-type species, and

$$\mu(z) = \mu^0(z) + \mu'(z) = \mu^0(z) + RT\ln a(z) \quad (3)$$

where a, μ^0 and μ' correspond to the activity, concentration-independent and concentration-dependent parts of the chemical potential, respectively. Statistical thermodynamics of solids

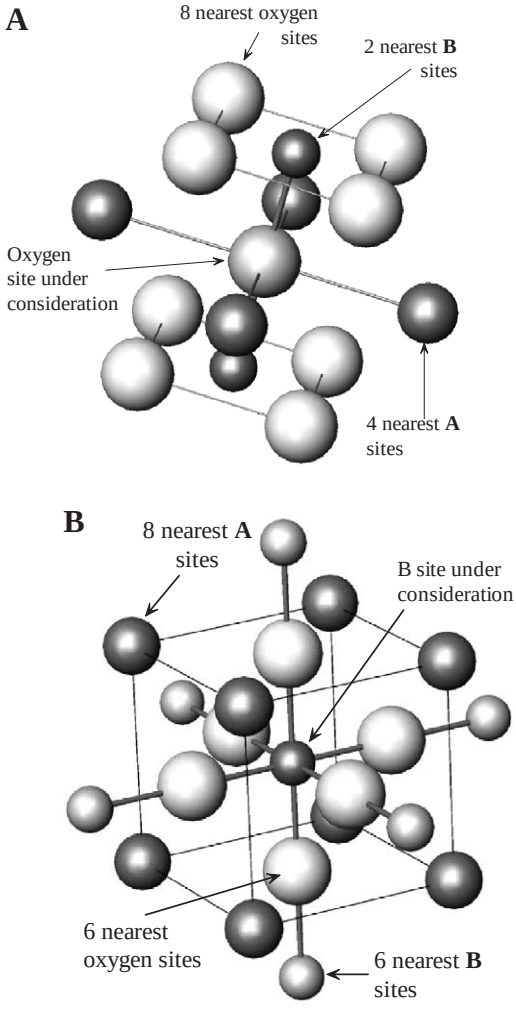

Fig. 1. Coordination of oxygen anions (A) and B-site cations (B) in the cubic perovskite lattice.

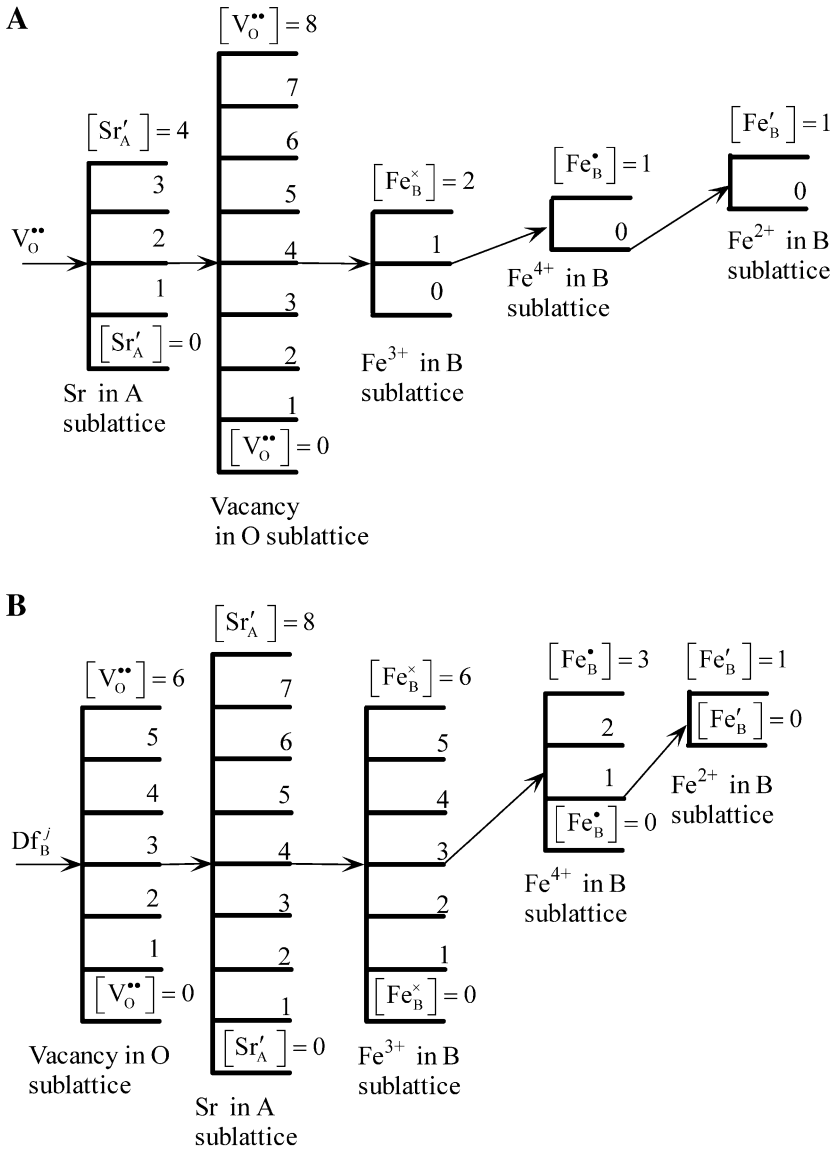

Fig. 2. Schematic illustration of the energy level splitting for oxygen vacancy (A) and B-site defect (B).

shows that, for structural elements in each sublattice of ABO_3 perovskite structure, the chemical potentials are uniquely related to each other and cannot be analyzed separately [17,29,30]. Since equilibrium concentrations of all components of the lattice are interrelated by the electroneutrality and site conservation conditions, a strict fulfillment of the definition of chemical potential as partial derivative of the free energy with respect to the particle concentration is impossible; the use of μ quantities to describe structural elements is hence associated with a number of assumptions and theoretical limitations [17,29,30]. One particular consequence is that the chemical potential of oxygen vacancies should be considered with respect to oxygen ions. For ideal solid solutions, all oxygen sites are equivalent:

$$\mu\left(V_o^{\bullet\bullet}\right) = \mu^0\left(V_o^{\bullet\bullet}\right) + RT\ln\frac{\left[V_o^{\bullet\bullet}\right]}{\left[O_o^{\times}\right]} \tag{4}$$

where the quantities in square brackets correspond to the concentrations related to one perovskite formula unit. In the case of non-ideal solid solutions, the concentrations in Eq. (4) should be corrected taking into account the energetic non-equivalence of the oxygen sites; particular cases are considered below. Nonetheless, the numbers of occupied and vacant sites are both comprised by the vacancy chemical potential, and Eq. (2) can be written as

$$\frac{\mu(O_2)}{RT} = 2\left(-\frac{\left(\Delta H_{ex} - \frac{1}{2}h^0_{O_2}\right) - T\left(\Delta S_{ex} - \frac{1}{2}s^0_{O_2}\right)}{RT} - \ln a\left(V_o^{\bullet\bullet}\right) + 2\ln a\left(h_B^{\bullet}\right)\right) \tag{5}$$

where the quantities ΔH_{ex} and ΔS_{ex} are related to one oxygen atom leaving the lattice, and the standard enthalpy and entropy

of gaseous molecular oxygen, $h^0_{O_2}$ ($J \times mol^{-1}$) and $s^0_{O_2}$ ($J \times mol^{-1} \times K^{-1}$), are defined according to the IUPAC data [31]:

$$h^0_{O_2} = R\left(3.5T + \frac{2271.15}{\exp(2243/T) - 1} - 1045\right) \quad (6a)$$

$$s^0_{O_2} = R\left(3.5\ln(T) + 4.725 + \frac{2271.15}{T(\exp(2243/T) - 1)} - 1.013\cdot\ln(1 - \exp(-2243/T))\right) \quad (6b)$$

2.2. Non-ideality of solid solutions: effects on the defect activity

Preliminary analysis of the $p(O_2)$-T-δ diagrams of $La_{0.3}Sr_{0.7}Fe_{1-x}Ga_xO_{3-\delta}$ under oxidizing conditions [18] showed inadequacy of the ideal solution model, suggesting that defect interactions and/or association cannot be neglected. In particular, the nearest neighborhood properties and the probability of placing a defect in the vicinity of other charged species should be considered. Similar studies were made by Ling [32], who developed a statistical-thermodynamic approach accounting for coulombic interactions and configurational entropy-related exclusion effects. The adequacy of the latter model, used to describe the behavior of CeO_2- and $LaCrO_3$-based phases, is however limited, especially in conditions where the deviations from stoichiometry are high [32–34]. In this work, the site-exclusion concept was enhanced introducing the defect interaction energy.

As starting hypothesis, it was assumed that some types of point defects cannot occupy neighboring sites in the lattice; these defects were identified from the atomistic simulation results. Another assumption was that each defect can be characterized using the ground energy level (E_0), common for all defects of this type. The value of E_0 corresponds to the minimum energy of this defect at a given temperature; the defect energy is assumed equal to E_0 when no other defects are present in the neighborhood, whilst the interaction with neighboring defects alters the

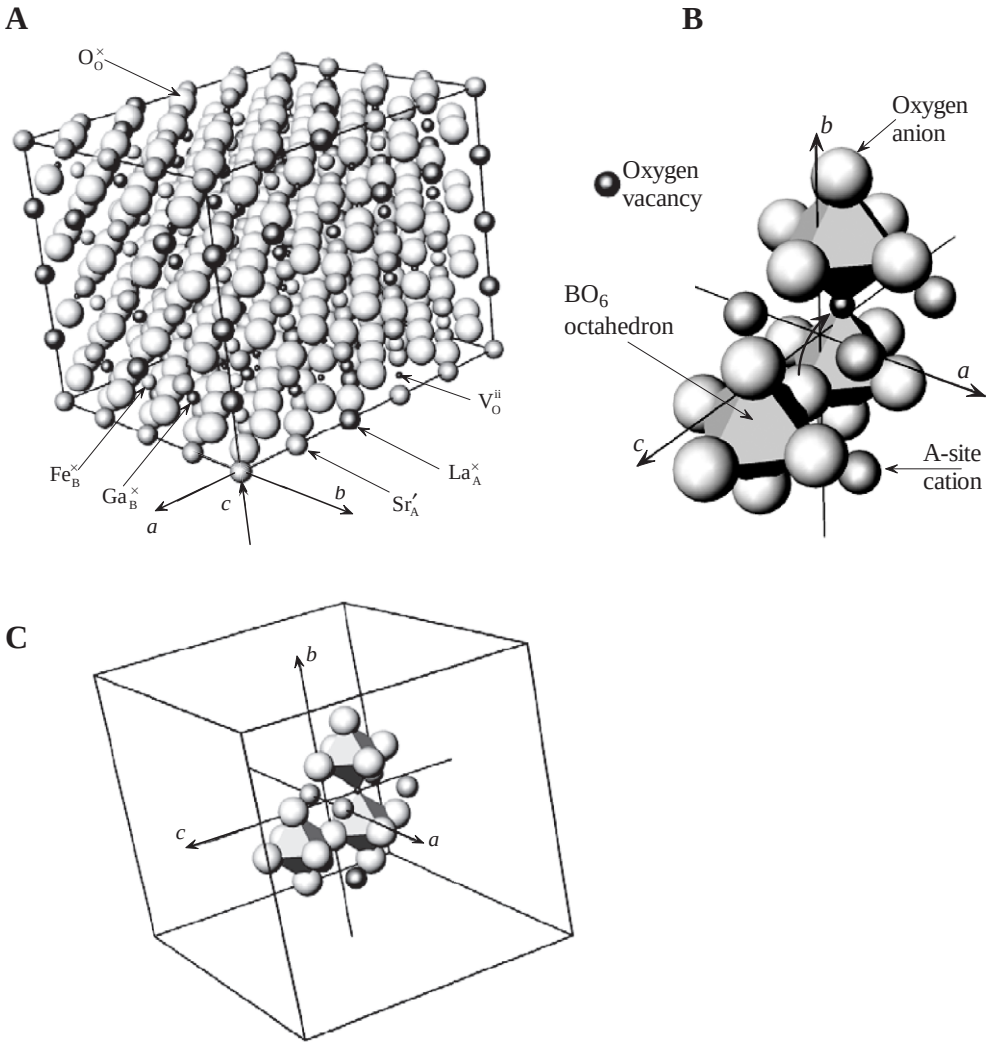

Fig. 3. Basic supercell used for the static lattice simulations (A), structural element critically affecting two central oxygen ions marked by arrow (B), and its placement in the supercell (C).

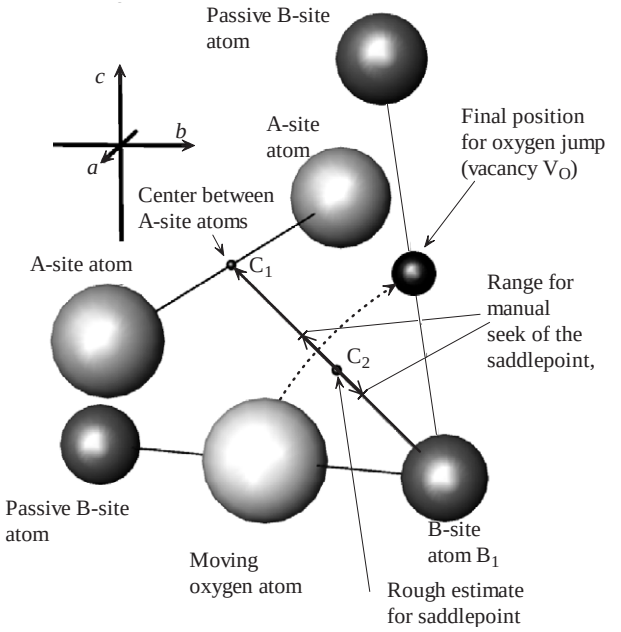

Fig. 4. Assessment of the ion migration pathway (see text).

energy. The relationships between the concentration of B-site defects, namely, electrons or holes, and their chemical potential were described in terms of the Fermi–Dirac distribution in discrete form:

$$\left[\mathrm{Df}_\mathrm{B}^j\right] = \sum_{k=0}^{N_k} \frac{N\left(\mathrm{Df}_\mathrm{B}^j, k\right)}{\exp\left[\dfrac{\left(E_k^0 + E_k\right) - \mu\left(\mathrm{Df}_\mathrm{B}^j\right)}{RT}\right] + q_n} \tag{7}$$

where Df_B^j corresponds to point defects with the charge j, the k index denotes their neighborhood, E_k is the corresponding energy level given with respect to the ground level E_k^0, $N(\mathrm{Df}_\mathrm{B}^j, k)$ is the number of states on the k level, and q_n is a spin-determined constant. In the given case, $q_n = 1$. The discrete density of states can be calculated from the probability of different configurations of the neighborhood, whereas the values of E_k can be assessed summing the contributions from all surrounding species to the energy level of a given defect.

For a cubic perovskite cell, each oxygen site is surrounded by 4 A-site ions, 2 cations in the B sublattice and 8 oxygen anions (Fig. 1). In the case of B-site cations, these coordination numbers are 8, 6 and 6, respectively. The corresponding structure of the energy levels in (Sr,La)(Fe,M')$O_{3-\delta}$ perovskites is presented in Fig. 2. Although a formal application of this structure to the distribution described by Eq. (7) results in excessively complex expressions for point-defect chemical potentials, the difference in the impact of some cations, e.g. La^{3+} and Sr^{2+} in the A sublattice, was found insignificant. Furthermore, a number of energy levels can be excluded from the distribution. For example, as shown below, the presence of more than one vacancy in the B–O octahedra of the perovskite structure is energetically unlikely, leading to the lattice reconstruction.

The ground energy level of Fe^{4+} was considered as $\mu^0(h_\mathrm{B}^\bullet)$ and thus included in the thermodynamic functions ΔH_{ex} and ΔS_{ex}, Eq. (5). Taking into account Eq. (3), the hole concentration and activity are related as

$$\left[\mathrm{Fe}_\mathrm{B}^\bullet\right] = a\left(h_\mathrm{B}^\bullet\right) \sum_{k=0}^{N_k} \frac{N\left(\mathrm{Fe}_\mathrm{B}^\bullet, k\right)}{\exp\left[\dfrac{E_k}{RT}\right] + a\left(h_\mathrm{B}^\bullet\right)} \tag{8}$$

The partition of Fe cations between the energy levels $N(\mathrm{Fe}_\mathrm{B}^j, k)$, shown in Fig. 2B, was assessed based on the iron neighborhood, assuming a statistical distribution of defects in the lattice. The contribution from each type of defects of a given sublattice (S2) into the density of states of a defect in the same or another sublattice (S1) can be calculated analyzing the corresponding probabilities, determined by the binomial distribution:

$$p(\mathrm{Df}_{S1}, M, n, m) = \binom{n}{m} \left(\frac{\left[M_{S2}^\times\right]}{F(M, S2)}\right)^m \left(1 - \frac{\left[M_{S2}^\times\right]}{F(M, S2)}\right)^{n-m} \tag{9}$$

where Df_{S1} is the defect under consideration, M_{S2} is the particular neighboring ion in the S2 subblatice, $F(M, S2)$ is the number of M species per perovskite unit formula, n is the coordination number, m is the number of M-type atoms

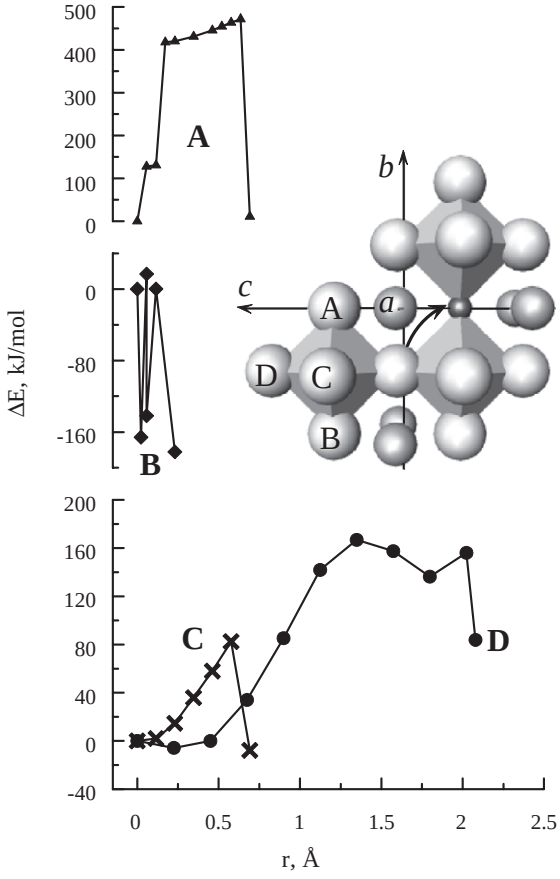

Fig. 5. Energy variations for oxygen ion moving towards a vacancy as shown by arrow in the inset, as function of the distance from initial equilibrium point. The calculations were made using the atomistic modelling technique, for the example of $La_{0.3}Sr_{0.7}Fe_{0.6}Ga_{0.4}O_{2.65}$. The cases A, B, C and D relate to the situations when another oxygen vacancy is placed in the correspondingly marked oxygen sites (see text).

neighboring the given Df_{S1} defect having the k-level energy, and $\binom{n}{m}$ is the binomial coefficient. For example, if the neighborhood of one Fe cation includes two Ga ions

$$p\left(\mathrm{Fe}, \mathrm{Ga}_B^{\times}, 6, 2\right) = \binom{6}{2}\left[\mathrm{Ga}_B^{\times}\right]^2\left(1-\left[\mathrm{Ga}_B^{\times}\right]\right)^4 \quad (10)$$

The total number of states for a k-level can be calculated as the product of partial probabilities:

$$N\left(\mathrm{Df}_{S1}^{j}, k\right) = \left[\mathrm{Df}_{S1}^{\Sigma}\right] \prod_i p\left(\mathrm{Df}_{S1}, M_i, n, m\right) \quad (11)$$

where $[Df_{S1}^{\Sigma}]$ is the total number of S1 sites, which can be occupied by this type of defects. As an example, for Fe^{4+}, the density of states with the k-level energy is

$$\begin{aligned} N\left(\mathrm{Fe}_B^{\bullet}, k\right) = {} & \left[\mathrm{Fe}_{\Sigma}\right] p\left(\mathrm{Fe}_B^{\bullet}, \mathrm{V}_o^{\bullet\bullet}, 6, 1\right) p\left(\mathrm{Fe}_B^{\bullet}, \mathrm{Sr}_A', 8, 4\right) \\ & \times p\left(\mathrm{Fe}_B^{\bullet}, \mathrm{Fe}_B^{\times}, 6, 3\right) \times p\left(\mathrm{Fe}_B^{\bullet}, \mathrm{Fe}_B^{\bullet}, 6, 1\right) \\ & \times p\left(\mathrm{Fe}_B^{\bullet}, \mathrm{Fe}_B', 6, 0\right) \end{aligned} \quad (12)$$

Attempts to describe experimental $p(O_2)$-T-δ diagrams of $La_{0.3}Sr_{0.7}Fe(M')O_{3-\delta}$, combining Eqs. (7) and (11) to express the point defect activity, failed due to a great number of formally different defect configurations. In fact, all models derived directly from this formalism were found statistically degenerated. This makes it necessary to discriminate all energetically impossible configurations and to exclude formal difference between the configurations having very similar energy. For these goals, the atomistic modelling technique [25–28] was used.

3. Atomistic simulations

The description of the atomistic simulation technique and its application to perovskite-type oxides was published elsewhere [25–27]. These calculations are based on the Born model for ionic solids; the charge of ions is considered equal to their formal oxidation state. The interactions between the ions are formulated in terms of long-range coulombic forces and two types of short-range interactions, namely the Pauli repulsion and van der Waals dispersion. The short-range forces are modelled using a standard Buckingham potential:

$$V_{ij} = A_{ij}\exp\left(-\frac{r}{\rho_{ij}}\right) - C_{ij}r^{-6} \quad (13)$$

where A_{ij}, ρ_{ij} and C_{ij} are parameters assigned to ion–ion interactions. The interatomic potential parameters and the properties of ions were taken from previous studies of La-containing perovskites [35–37]; the simulations of the point defects in $La_{0.3}Sr_{0.7}Fe(M')O_{3-\delta}$ were based on Mott–Littleton approach. For the calculations, the potential cutoff radius and the region of most precise similations enabled by this technique (so-called A region) were selected as 12 and 10 Å, respectively. One necessary comment is that, although these values are large enough with respect to the atom displacements tested in this work, the use of atomistic modelling technique for highly disordered ferrite lattices is associated with important limitations. The corresponding uncertainties are primarily determined by covalent contributions to Fe–O bonding and tendencies to the local and long-range vacancy ordering processes. The data on crystal structure and electron-hole transport [12,18], indicating a small-polaron conduction mechanism, suggest that these uncertainties should be mild. Nonetheless, the simulation results were used for qualitative conclusions only.

Modelling of the solid solutions, where a sublattice may comprise up to 15–20% defects [12,18], requires the use of a supercell approach. The supercell comprising a number of perovskite formula units is considered as the primitive structural element, built on the basis of structural data [12,21]. Taking into account the concentration ranges of oxygen vacancies, holes and M' dopants [18], the final supercell size was selected as $5\times4\times4$ perovskite cells, with 80, 80 and 240 sites in the A, B and oxygen sublattices, respectively (Fig. 3A). The ions are distributed randomly, with simultaneous discrimination of energetically unfavorable configurations.

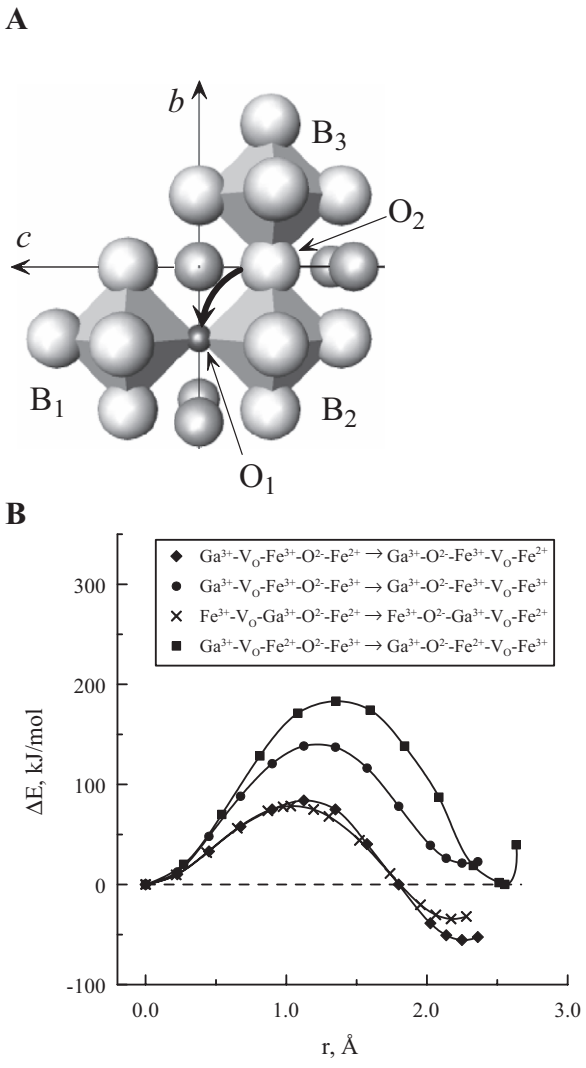

Fig. 6. Structural element illustrating the assessment of Fe_B'–$V_o^{\bullet\bullet}$ pair cluster formation (A), and the energy variations for 4 typical configurations where one oxygen vacancy moves around various B sites (B). The initial and final configurations of the B_1–O_1–B_2–O_2–B_3 sites are given in the legend. The calculations were made using $La_{0.3}Sr_{0.7}Fe_{0.6}Ga_{0.4}O_{2.65}$ as model composition.

Table 1
Energetic effect for the placement of electron hole in the oxygen vacancy neighborhood, for the example of $La_{0.3}Sr_{0.7}Fe_{0.6}Ga_{0.4}O_{2.65}$

State of the structural element shown in Fig. 6A*		Transition energy, kJ/mol
Initial	Final	
$Ga^{3+}-V_O-Fe^{3+}-O^{2-}-Fe^{4+}$	$Ga^{3+}-V_O-Fe^{4+}-O^{2-}-Fe^{3+}$	23.8
$Fe^{3+}-V_O-Fe^{3+}-O^{2-}-Fe^{4+}$	$Fe^{3+}-V_O-Fe^{4+}-O^{2-}-Fe^{3+}$	16.5

* See text for details.

The simulations revealed that the occupancy of two oxygen sites, placed at the edge of a metal-oxygen octahedron, and the energy of the corresponding configurations are critically dependent on the presence of point defects in crystallographic sites shown in Fig. 3B. This local zone, comprising four nearest A-site cations and at least three B–O octahedra, was therefore used for the analysis of possible configurations; its relative position in the supercell used for the calculations is illustrated by Fig. 3C. The occupation of all other sites in each sublattice was random, except for the mass conservation condition and for the following limitations: (i) the distance between oxygen vacancies should be as great as possible; (ii) Fe^{4+} cannot be statically placed near an oxygen vacancy; (iii) the preferable position of Fe^{2+} is in the vacancy neighborhood.

One particular method, used to exclude energetically unfavorable configurations involving oxygen vacancies, relates to the simulations of ion migration. For several specific defect configurations, placing a vacancy into a specific oxygen site results in complete reconstruction of the structure. As this situation cannot be modelled using the static lattice approach, these unlikely configurations were assessed shifting one oxygen ion from equilibrium position in a critical direction, along which the complete jump would result in the lattice instability. The energy increment at the lability point was considered as stability limit of a given defect configuration. On the other hand, massive deformations were observed in $La_{0.3}Sr_{0.7}Fe(M')O_{3-\delta}$ lattice near $Fe_B^{\bullet}-V_o^{\bullet\bullet}$ pair clusters and isolated divalent iron cations, and also when the distance between oxygen vacancies was shorter than a certain limit close to the cubic perovskite unit cell parameter (~3.9 Å). In such cases, the modified procedure included building a B_1C_1 vector (Fig. 4), the center of which (C_2) was considered as a first approximation for further calculations of real saddle-point; then a series of calculations with fixed interstitial positions was carried out to detect the saddle-point manually, with simultaneous adjustment of the most likely oxygen-migration pathway.

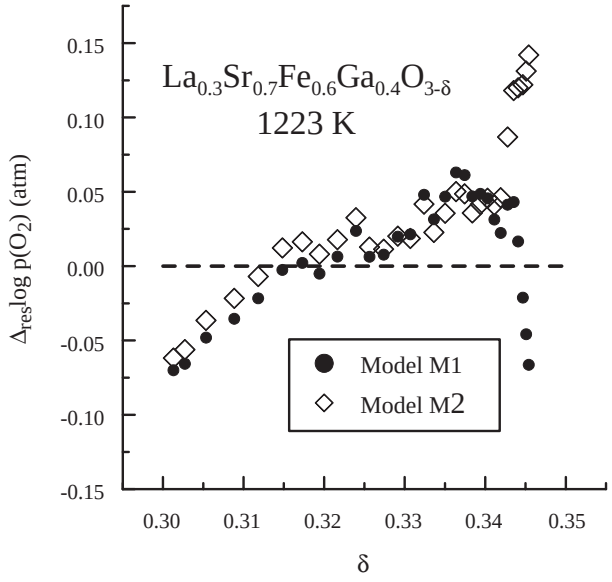

Fig. 7. Example of the fitting residuals distribution for the M1 and M2 models.

The results showed that the presence of two oxygen vacancies in one metal-oxygen octahedron is energetically unfavorable. As an example, Fig. 5 presents the energy variations related to one oxygen anion moving towards a vacancy as marked by the arrow; the situations denoted as A, B, C and D correspond to the cases when another oxygen vacancy is present in the respective oxygen sites. In the cases A, B and C, completing this jump would result in the formation of two neighboring vacancies at the edge of metal–oxygen octahedron; in the case D, the vacancies would occupy opposite corners. However, in all these situations, no vacancy pair can be formed. For the cases A, C and D, the ion movement is accompanied with a jump of the second oxygen vacancy in a more distant site, reflected by the energy drop (Fig. 5). Necessary to note the extreme values of the transition-state energy are observed in the situation A, suggesting that the oxygen ion placed between two vacancies cannot move towards any of them. Similar conclusion is drawn analyzing the situation B, when all three oxygen sites under consideration are placed in line. In the latter case, the lattice becomes unstable immediately after the oxygen ion leaves its equilibrium position between two

Table 2
Parameters of the regression models for $p(O_2)$-T-δ diagram of $La_{0.3}Sr_{0.7}Fe(M')O_{3-\delta}$

Parameter	$x=0$		$x=0.2$, $M'=$Ga	$x=0.4$, $M'=$Ga		$x=0.2$, $M'=$Al	$x=0.4$, $M'=$Al
	Model M1	Model M2	Model M1	Model M1	Model M2	Model M2	Model M1
ΔH_{ex}, kJ/mol	92±2	92±2	90±1	76.4±0.7	78.7±0.9	87.2±0.8	79±1
ΔS_{ex}, J/mol×K	−59±2	−57±1	−44±1	−46.3±0.6	−46.4±0.9	−51.6±0.6	−45±1
ΔE ($Fe_B^{\bullet}\rightarrow Fe_B^{\bullet}$), kJ/mol	2.4±0.2	2.4±0.1	2.3±0.1	3.0±0.2	4.0±0.2	4.09±0.07	5.6±0.4
ΔH_{pn}, kJ/mol	*	–	63±2	67±1	–	–	67±3
Adjusted correlation coefficient	0.9993	0.9993	0.9991	0.9997	0.9993	0.9995	0.9989
Relative error, %	0.8	0.8	0.9	0.5	0.8	0.7	1.0
Number of data points	141	141	184	202	202	198	192

The parameter was statistically insignificant.

vacancies; this movement shifts the C-position anion up to 0.78 Å from its original placement, followed by the B-position vacancy jump as observed in the previous cases. Thus, all configurations, where the distance between two vacancies corresponds to one elementary ion jump, are energetically unlikely and excluded from the defect chemistry analysis of the title materials. Note that the latter conclusion should be considered as only applicable to perovskite-type $La_{0.3}Sr_{0.7}Fe(M')O_{3-\delta}$ (M' = Ga, Al), and under oxidizing conditions only. The favorable defect configurations in B-site substituted ferrites depend significantly on the composition of the A sublattice and on the oxygen nonstoichiometry. As a particular example, for $SrFe(Al)O_{3-\delta}$ perovskites the location of two oxygen vacancies near Al^{3+} cation, forming aluminum–oxygen tetrahedron, was found energetically favorable; the results will be summarized in a separate publication. Such difference in behavior, probably associated with changing the positive charge density in the lattice, suggests that any extrapolation of the above conclusions to other ferrite-based materials requires further experimental validation.

The formation of localized electrons, Fe^{2+} or Fe'_B, is characteristic of $La_{0.3}Sr_{0.7}Fe(M')O_{3-\delta}$ solid solutions under reducing conditions, when the generation of n-type electronic charge carriers is confirmed by data on the total conductivity, Seebeck coefficient and oxygen nonstoichiometry [11,12,18]. The coulometric titration results presented below indicate also significant deviations in the $p(O_2)$-δ isotherms under moderately oxidizing conditions, at $p(O_2) = 10^{-5} - 10^{-4}$ atm, which cannot be adequately described neglecting electrons. However, if even the presence of significant concentrations of Fe^{2+} is assumed in combination with holes as dominant electronic charge carriers, the resultant thermodynamic parameters for iron disproportionation contradict all experimental data on Fe-containing materials ([2,8,13] and references cited). Such a behavior can be explained assuming the formation of $Fe'_B - V_o^{\bullet\bullet}$ pair associates, which seems to be in agreement with the effective charge of these defects, ionic radius of Fe^{2+}, relatively low mobility of the n-type charge carriers in ferrites and high activation energy for their migration [8,38]. This hypothesis was also confirmed in the course of the atomistic simulations.

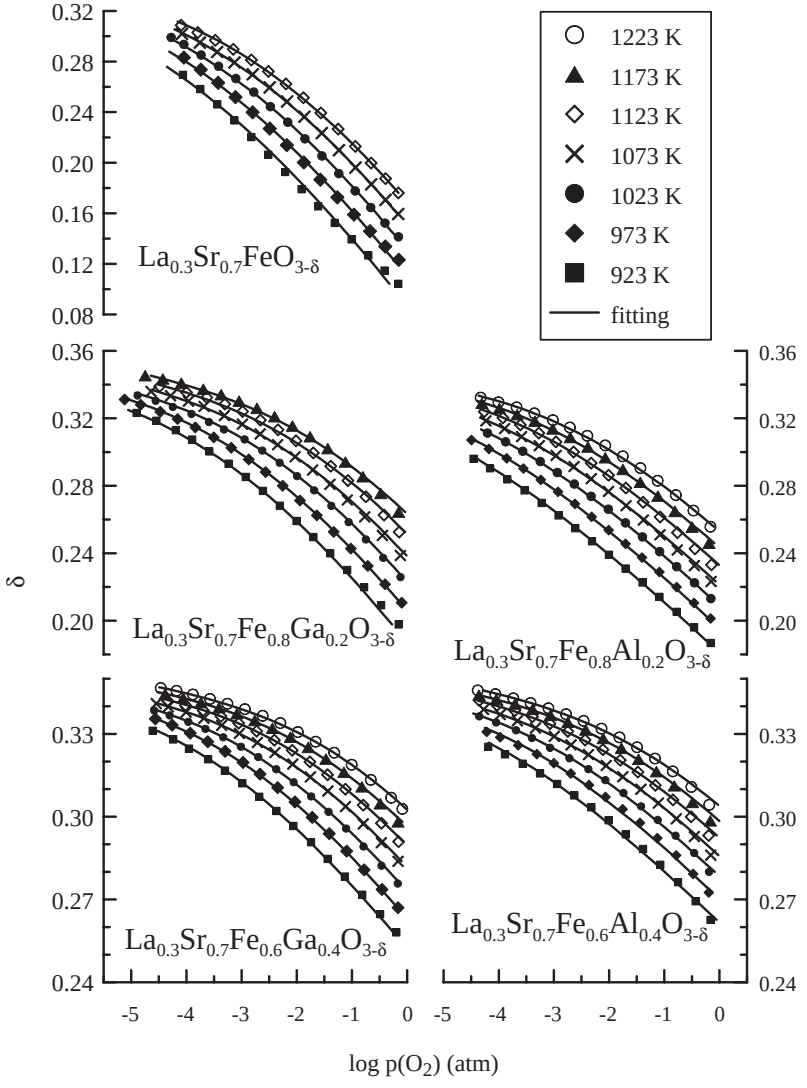

Fig. 8. The $p(O_2)$-T-δ diagrams of $La_{0.3}Sr_{0.7}Fe(M')O_{3-\delta}$. Solid lines correspond to the fitting results.

The simulations of $Fe'_B - V_o^{\bullet\bullet}$ clusters were performed moving one vacancy between two different neighborhoods, using one structural element (Fig. 6A) similar to that shown in Fig. 3C. Fig. 6B illustrates the energy variations for four typical configurations. In all cases, the vacancy was moved from the O_1 site, surrounded by the B_1 and B_2 cations, into the O_2 position as denoted in Fig. 6A. The results clearly show that placing a vacancy near Fe^{2+} is energetically beneficial with respect to the configurations involving trivalent surrounding, either Ga^{3+} or Fe^{3+}, the latter being less favorable. The vacancy jump around Fe^{2+} has no essential energetic effect. These estimations suggest that the formation of $Fe'_B - V_o^{\bullet\bullet}$ pair clusters should lead to a substantial decrease of the lattice energy, thus making unlikely the presence of stable Fe^{2+} in isolated state.

No lattice instabilities were detected when a hole is located in the nearest neighborhood of one oxygen vacancy, although both defects are positively charged. Nevertheless, the defect configurations comprising neighboring Fe^{4+} and vacancies are energetically unfavorable; two representative examples are given in Table 1. Due to the low activation energies for hole mobility in $La_{0.3}Sr_{0.7}Fe(M')O_{3-\delta}$ [12,18], static existence of such configurations seems unlikely.

4. Model formulation

For the mobile charge carriers, holes and oxygen vacancies, more than 30 likely configurations of the surrounding cations in the A and B sublattices were tested. The difference in the influence of A-site cations, La^{3+} and Sr^{2+}, on point defect activity was found negligible. As an example, when a hole jumps from an iron cation surrounded by strontium only into the site neighbored by 4 La^{3+} and 4 Sr^{2+} ions, the energetic effect is about 5 kJ/mol, close to the background level. For holes, only the presence of other holes in the neighborhood leads to the energy level splitting. In the case of oxygen vacancies and electrons, no splitting was confirmed statistically; these have also no effect on the separation of hole energy levels. Therefore, Eq. (9) can be written as

$$p\left(Fe_B^{\bullet}, V_o^{\bullet\bullet}, 6, 0\right) = \binom{6}{0}\left(\frac{\left[V_o^{\bullet\bullet}\right]}{3}\right)^0\left(1-\frac{1}{3}\left[V_o^{\bullet\bullet}\right]\right)^6 = \left(1-\frac{1}{3}\left[V_o^{\bullet\bullet}\right]\right)^6 \tag{14}$$

$$p\left(V_o^{\bullet\bullet}, Fe_B^{\bullet}, 2, 0\right) = \binom{2}{0}\left[Fe_B^{\bullet}\right]^0\left(1-\left[Fe_B^{\bullet}\right]\right)^2 = \left(1-\left[Fe_B^{\bullet}\right]\right)^2 \tag{15}$$

for the holes and vacancies, respectively. For the density of states

$$N\left(Fe_B^{\bullet}, i, j\right) = [Fe_{av}]p\left(Fe_B^{\bullet}, V_o^{\bullet\bullet}, 2, 0\right) \times p\left(Fe_B^{\bullet}, Fe_B^{\times}, 6, i\right)p\left(Fe_B^{\bullet}, Fe_B^{\bullet}, i, j\right) \tag{16}$$

where $[Fe_{av}]=[Fe_\Sigma]-[Fe'_B]$ is the number of sites available for the holes, $[Fe_\Sigma]$ is the total concentration of iron related to one perovskite formula unit, i and j are the numbers of Fe^{3+} and Fe^{4+} cations in the nearest neighborhood of the hole under consideration, respectively.

The energy of each hole level was considered as a linear function of the environment contributions:

$$E_{i,j} = \sum_{i=0}^{6}\sum_{j=0}^{i}\left[i\Delta E\left(Fe_B^{\times}\rightarrow Fe_B^{\bullet}\right) + j\Delta E\left(Fe_B^{\bullet}\rightarrow Fe_B^{\bullet}\right)\right] \tag{17}$$

where $\Delta E(Fe_B^{\times}\rightarrow Fe_B^{\bullet})$ and $\Delta E(Fe_B^{\bullet}\rightarrow Fe_B^{\bullet})$ are the interaction energies between Fe^{3+} and Fe^{4+}, and between holes, respectively. The former quantity was statistically insignificant in all cases, enabling to simplify Eq. (17):

$$E_{i,j} = \sum_{i=0}^{6}\sum_{j=0}^{i} j\Delta E\left(Fe_B^{\bullet}\rightarrow Fe_B^{\bullet}\right) \tag{18}$$

Thus, the holes were found to possess 7 actual energy levels, with a kind of degeneration induced by the resemblance between Fe^{3+}, Ga^{3+} and Al^{3+} cations having similar charge.

As no splitting of the energy levels was confirmed for the vacancies,

$$N\left(V_o^{\bullet\bullet}, 1\right) = [O_\Sigma]p\left(V_o^{\bullet\bullet}, V_o^{\bullet\bullet}, n_V, 0\right)p\left(V_o^{\bullet\bullet}, Fe_B^{\bullet}, 2, 0\right) \tag{19}$$

The term $p(V_o^{\bullet\bullet}, V_o^{\bullet\bullet}, n_v, 0)$ means that no other vacancies can occupy the vacancy-neighboring oxygen sites, the number of which corresponds to the coordination number n_V. In the course of calculations, several versions of n_V values were tested, including 8 (nearest neighborhood, Fig. 1A), 10 (all oxygen sites comprising two nearest B–O octahedra), 12 (nearest neighborhood and 4 sites closest across the O–A–O bonds), and 14 (all listed positions). The models with $n_V=8$ were found most adequate. Therefore, the oxygen vacancy chemical potential can be expressed directly as

$$\mu'\left(V_o^{\bullet\bullet}\right) = RT\ln\frac{\left[V_o^{\bullet\bullet}\right]}{N\left(V_o^{\bullet\bullet}, 1\right) - \left[V_o^{\bullet\bullet}\right]} \tag{20}$$

Taking into account the atomistic modelling results, the formation of Fe^{2+} in $La_{0.3}Sr_{0.7}Fe(M')O_{3-\delta}$ under oxidizing conditions should result in the $Fe'_B - V_o^{\bullet\bullet}$ pair clusters following the iron disproportionation reaction:

$$V_o^{\bullet\bullet} + 2Fe_B^{\times}\langle V_o\cdots Fe_B\rangle^{\bullet} + Fe_B^{\bullet} \qquad K_{pn} = \frac{a\left(\langle V_o\cdots Fe_B\rangle^{\bullet}\right)a\left(Fe_B^{\bullet}\right)}{a\left(V_o^{\bullet\bullet}\right)} \tag{21}$$

The chemical potential of these clusters, denoted as $\langle V_o \cdots Fe_B\rangle^{\bullet}$, may be derived as

$$\mu'\left(\langle V_o\cdots Fe_B\rangle^{\bullet}\right) = RT\ln\frac{\left[\langle V_o\cdots Fe_B\rangle^{\bullet}\right]}{N\left(\langle V_o\cdots Fe_B\rangle^{\bullet}, -1\right) - \left[\langle V_o\cdots Fe_B\rangle^{\bullet}\right]} \tag{22}$$

with

$$N\left(\langle V_o\cdots Fe_B\rangle^{\bullet}, -1\right) = \left([Fe_\Sigma]-[Fe'_B]\right) \times \left(1-p\left(\langle V_o\cdots Fe_B\rangle^{\bullet}, V_o^{\bullet\bullet}, 6, 0\right)\right) \tag{23}$$

where the term $[1-p(\langle V_o \cdots Fe_B\rangle^{\bullet}, V_o^{\bullet\bullet}, 6, 0]$ implies that at least one vacancy should be present near Fe^{2+}. The low concentration of electrons under oxidizing conditions, studied in this work,

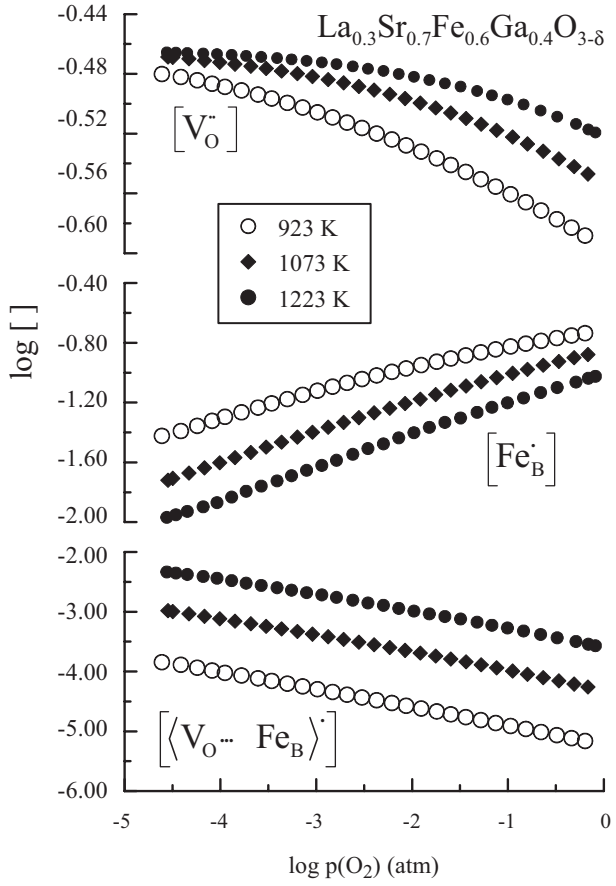

Fig. 9. Oxygen partial pressure dependencies of the calculated defect concentrations in $La_{0.3}Sr_{0.7}Fe_{0.6}Ga_{0.4}O_{3-\delta}$.

limits the possibility for further improvement of this model, until the low-p(O_2) range is investigated. Nonetheless, the presence of electron-vacancy clusters was statistically confirmed for $La_{0.3}Sr_{0.7}Fe_{0.6}M'_{0.4}O_{3-\delta}$ (M' = Al, Ga) and $La_{0.3}Sr_{0.7}Fe_{0.8}Ga_{0.2}O_{3-\delta}$ perovskites. For two other ferrites, this effect is negligible.

The basic equations describing $La_{0.3}Sr_{0.7}Fe_{1-x}M'_xO_{3-\delta}$ defect chemistry include also the electroneutrality and site conservation conditions:

$$2\left[V_o^{\bullet\bullet}\right] + \left[\langle V_o \cdots Fe_B\rangle^{\bullet}\right] + \left[Fe_B^{\bullet}\right] = [Sr_B'] \quad (24)$$

$$\left[V_o^{\bullet\bullet}\right] + \left[\langle V_o \cdots Fe_B\rangle^{\bullet}\right] + \left[O_o^{\times}\right] = [O_\Sigma] = 3 \quad (25)$$

$$\left[\langle V_o \cdots Fe_B\rangle^{\bullet}\right] + \left[Fe_B^{\bullet}\right] + \left[Fe_B^{\times}\right] = [Fe_\Sigma] = 1 - x \quad (26)$$

Two models were finally selected as most adequate: with and without electrons. The model accounting for Fe^{2+} (Model M1) comprises Eqs. (5), (8), (16) and (20)–(26). For the simplified model (M2) neglecting n-type charge carriers, Eqs. (21)–(23) were excluded and Eqs. (23)–(26) were modified to skip the pair clusters.

5. Experimental methods

Powders and ceramics of perovskite-type $La_{0.3}Sr_{0.7}Fe_{1-x}Ga_xO_{3-\delta}$ (x = 0–0.4) were prepared by a standard ceramic route in air, as described elsewhere [11]. For the synthesis of $La_{0.3}Sr_{0.7}Fe_{1-x}Al_xO_{3-\delta}$ where the solid state reactions may be stagnated due to kinetic reasons, the glycine–nitrate process (GNP), a self-combustion technique using glycine as a fuel and nitrates of metal components as an oxidant, was used; experimental conditions of the GNP and ceramics sintering are found in Ref. [12]. Characterization of the title materials included X-ray diffraction (XRD) and neutron diffraction analysis, scanning electron microscopy combined with energy dispersive analysis (SEM/EDS), inductively coupled plasma spectroscopic analysis, and the measurements of total conductivity (4-probe DC) and Seebeck coefficient as a function of temperature and oxygen partial pressure; the oxygen ionic conductivity was calculated from the faradaic efficiency and oxygen permeability data. Detailed description of experimental techniques and equipment can be found in previous publications ([10–12,18,21] and references therein). The oxygen content variations with respect to a reference point were measured as function of oxygen partial pressure and temperature using the coulometric titration technique in double electrochemical cells [19]. For $La_{0.3}Sr_{0.7}FeO_{3-\delta}$, the total oxygen content in the reference state (1023 K, air) was determined by thermogravimetric analysis [18]. In all other

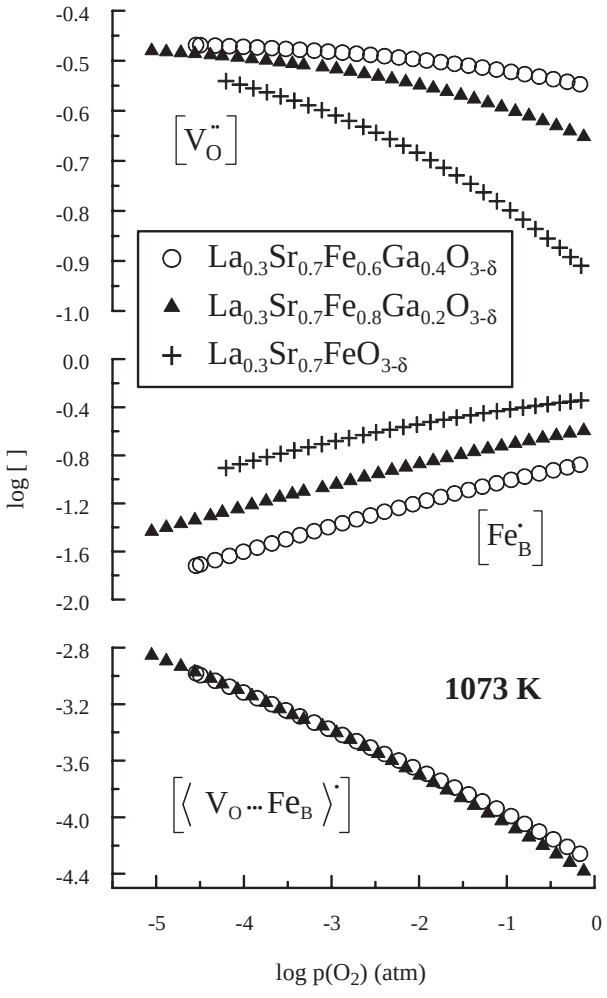

Fig. 10. Effect of the B-site dopant content on the defect concentrations.

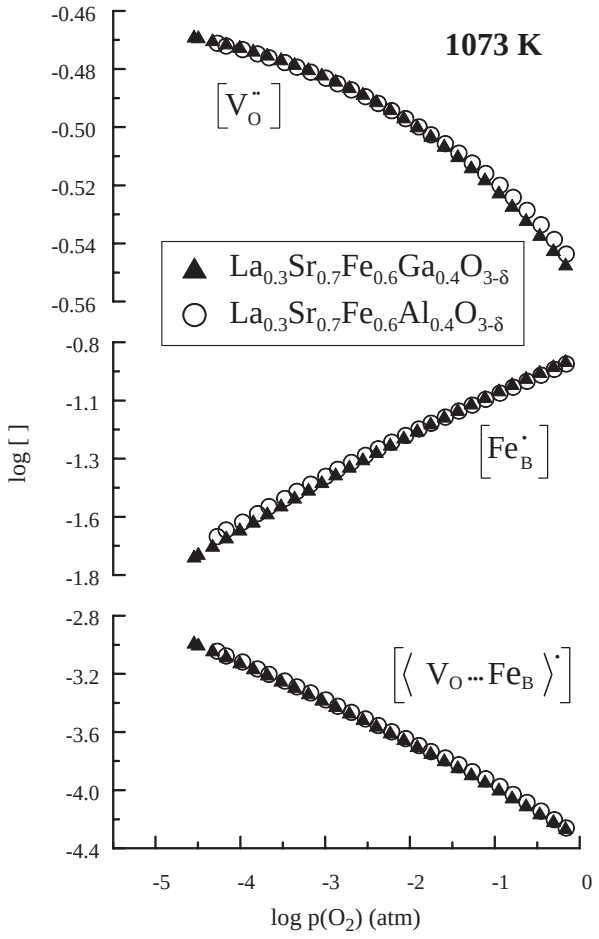

Fig. 11. Effect of the B-site dopant cations on the defect concentrations.

cases, the electron-hole equilibrium points at low p(O_2), where the average oxidation state or iron is 3+ and the total oxygen content is hence 2.65 per unit formula, were used as reference for the arrays of the coulometric titration data, as described elsewhere [18]. The nonlinear regression analysis procedure for fitting of the experimental data on oxygen nonstoichiometry was also reported earlier [39]. The models were formulated in the form

$$Y_i = 2\left(-\frac{\Delta H_{ex}}{RT_i} + \Delta S_{ex} - \ln a_v(\delta_i, T_i) + 2\ln a_h(\delta_i, T_i) \right) \quad (27)$$

with $Y_i = [\mu(O_2)_i - (h^0_{O_2} - T_i s^0_{O_2})]/RT_i$ being the dependent variable. The values of $\mu(O_2)_i$ were calculated from $p(O_2)_i$ and T_i using Eqs. (6a) (6b); the independent variables included δ_i and T_i.

6. Results and discussion

The models denoted as M1 and M2 result in very similar thermodynamic parameters (Table 2). In fact, their difference is close to the fitting errors. Nonetheless, comparison of the statistical parameters and analysis of the residuals distribution unambiguously showed that the contribution of $Fe'_B - V_o^{\cdot\cdot}$ pair clusters cannot be neglected for the Ga-substituted phases and $La_{0.3}Sr_{0.7}Fe_{0.6}Al_{0.4}O_{3-\delta}$. One representative example of the fitting residuals distribution is shown in Fig. 7. Although a correlation with δ values is observed for both models, this effect is considerably less pronounced in the case of M1 model, suggesting a significant role of the n-type electronic charge carriers. Similar conclusion can be drawn comparing the overall errors, Table 2. For $La_{0.3}Sr_{0.7}FeO_{3-\delta}$ and $La_{0.3}Sr_{0.7}Fe_{0.8}Al_{0.2}O_{3-\delta}$ perovskites, the contributions of pair clusters in oxygen thermodynamics are statistically insignificant.

The final fitting results of the p(O_2)-T-δ diagrams of $La_{0.3}Sr_{0.7}Fe_{1-x}M'_xO_{3-\delta}$ are shown in Fig. 8 as solid lines. The proposed models provide adequate descriptions of the oxygen nonstoichiometry changes within all the studied ranges of oxygen partial pressure and temperature. This makes it possible to analyze quantitatively the relative contributions of particular defect interactions.

The relationships between point defect concentrations, p(O_2), temperature and dopant content (Figs. 9 and 10) are quite predictable. Namely, the concentration of oxygen vacancies increases with increasing temperature and M' cation additions, and on reducing the oxygen chemical potential. The behavior of $Fe'_B - V_o^{\cdot\cdot}$ clusters is similar, except for an almost

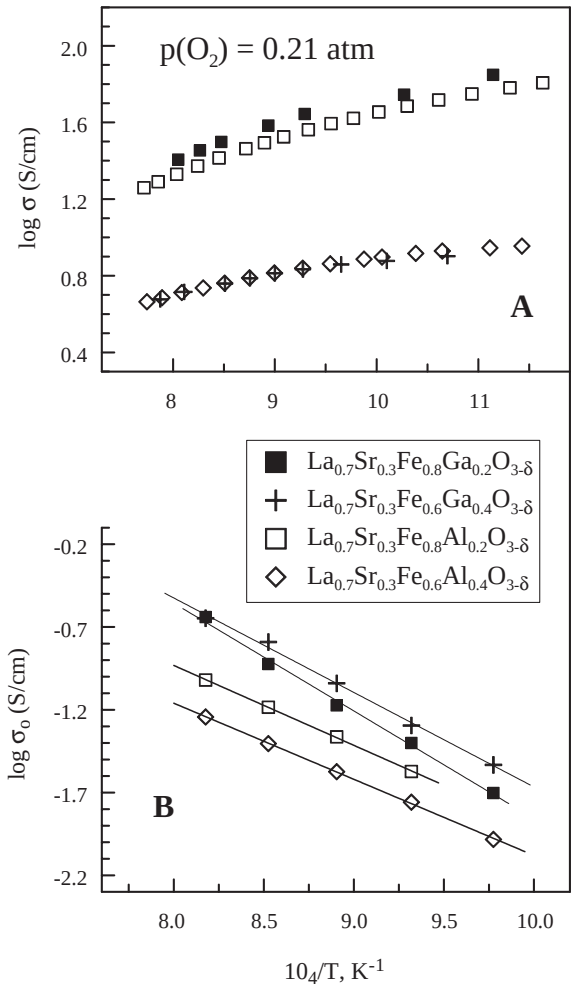

Fig. 12. Temperature dependence of the total (A) and partial oxygen ionic (B) conductivities of $La_{0.3}Sr_{0.7}Fe(M')O_{3-\delta}$.

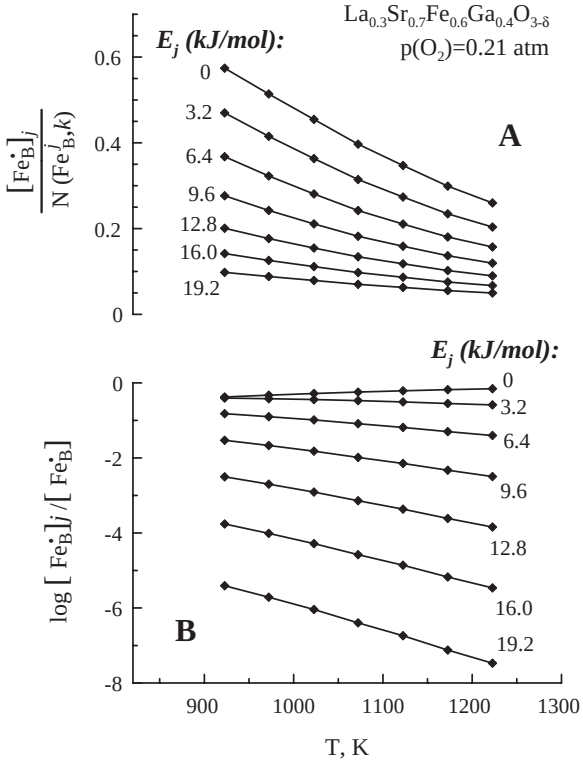

Fig. 13. Temperature dependencies of the occupancy of hole energy levels (A) and the distribution of holes between the levels (B) for $La_{0.3}Sr_{0.7}Fe_{0.6}Ga_{0.4}O_{3-\delta}$ in air.

negligible dependence on the dopant content; the holes exhibit opposite trends. The role of iron disproportionation process increases with temperature, as expected from thermodynamics. In all cases, the total defect concentrations in $La_{0.3}Sr_{0.7}Fe_{1-x}M'_xO_{3-\delta}$ perovskites with equal dopant content are quite similar, indicating a substantial similarity in the behavior of Ga^{3+} and Al^{3+} cations in the ferrite lattice (Fig. 11). This corresponds well to the data on total conductivity (Fig. 12A), which is predominantly p-type electronic [11,12,18] and depends primarily on the concentrations of Fe^{4+} and iron sites available for hole hopping. However, the ionic conductivity of Al-substituted ferrites is substantially lower with respect to the Ga-doped analogues (Fig. 12B).

Inspection of the energy level occupancies, $[Fe_B^{\bullet}]_j/N(Fe_B^j,k)$, and the hole distribution between the levels, $[Fe_B^{\bullet}]_j/[Fe_B^{\bullet}]$, reveals that for heavily doped $La_{0.3}Sr_{0.7}Fe_{1-x}M'_xO_{3-\delta}$ two states with the lowest energy are dominant (Figs. 13 and 14). These levels (E_0 and E_1) correspond to the situations where the nearest B-site neighborhood of Fe^{4+} comprises no other holes and one hole, respectively. The dominance of low-energy states becomes more pronounced when the temperature increases or the oxygen partial pressure decreases, due to decreasing total concentration of electron holes. At the same time, the overall pattern of hole distribution as a function of the M' cation concentration in $La_{0.3}Sr_{0.7}Fe_{1-x}M'_xO_{3-\delta}$ is more complex (Fig. 15). Decreasing dopant content leads to a considerably higher contribution of the moderate-energy levels, related to the states when two or more holes occupy the B sites surrounding Fe^{4+}. Also, the fraction of holes having the highest energy (E_5 and E_6) drastically increases with decreasing x; if comparing $La_{0.3}Sr_{0.7}Fe_{0.6}Ga_{0.4}O_{3-\delta}$ and $La_{0.3}Sr_{0.7}FeO_{3-\delta}$, the corresponding difference is as large as 10^5–10^6 times. The latter trends are also reflected by an increase in the hole-hole repulsive forces expressed via the $\Delta E(Fe_B^{\bullet} \rightarrow Fe_B^{\bullet})$ energy, on doping with gallium or aluminum (Table 2). One can conclude therefore that the incorporation of cations with stable oxidation state, such as Ga^{3+} or Al^{3+}, has a strong effect on the electronic sublattice of $La_{0.3}Sr_{0.7}Fe(M')O_{3-\delta}$ solid solutions, decreasing the covalency of Fe–O bonds and increasing the tendencies to hole localization and iron disproportionation.

The difference in the influence of Al^{3+} and Ga^{3+} cations on hole distribution (Fig. 16 and Table 2) is more significant than their effects on the total concentration of Fe^{4+} (Fig. 11). Namely, with respect to gallium doping, the presence of Al^{3+} in the perovskite lattice increases hole repulsion and thus promotes more isolated states of the holes. This tendency is clearly visible for the high-energy levels. Their occupation is up to 10 times higher for the Ga-substituted ferrites. Most likely, such behavior is due to smaller ionic radius of Al^{3+} compared to Ga^{3+}, resulting in greater local distortions of the perovskite lattice near dopant cations and, hence, higher ionicity of the B–O bonds in Al-containing phases. The local distortions of Al–O polyhedra and the higher repulsive forces between electron holes may be partly responsible for the

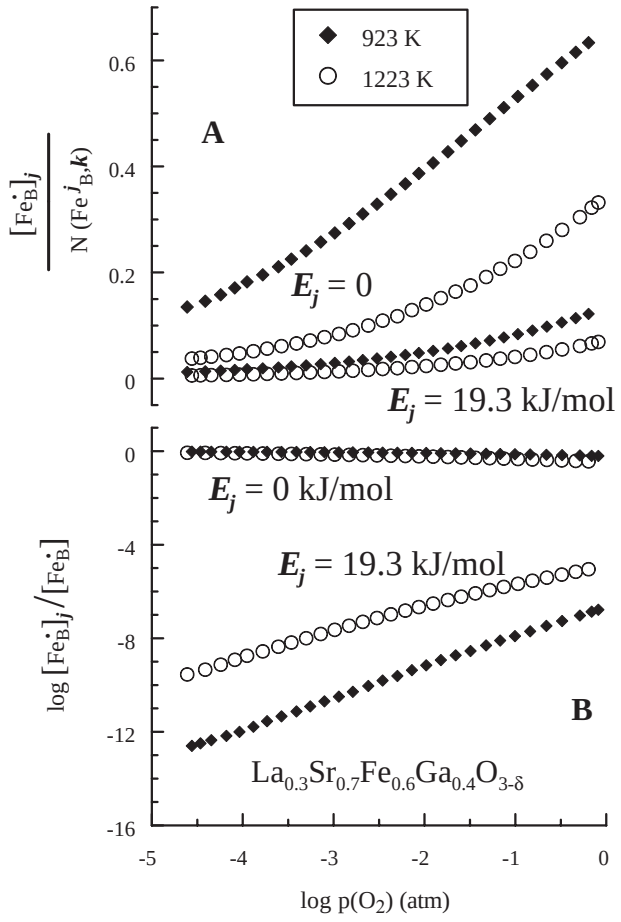

Fig. 14. Oxygen partial pressure dependence of the occupancy of hole energy levels (A) and the distribution of holes between the levels (B) for $La_{0.3}Sr_{0.7}Fe_{0.6}Ga_{0.4}O_{3-\delta}$ at 923 and 1223 K.

decrease in ionic conductivity, observed in $La_{0.3}Sr_{0.7}Fe_{1-x}Al_xO_{3-\delta}$ when x increases (Fig. 12). In particular, as close locations of an oxygen vacancy and Fe^{4+} are unlikely due to their coulombic interaction, an increasing tendency to the formation of Fe^{4+} isolated states should be associated with decreasing concentration of oxygen sites available for the vacancy jumps.

7. Conclusions

The atomistic simulations were used to identify energetically favorable point-defect configurations, which may influence the oxygen nonstoichiometry vs. $p(O_2)$ variations in perovskite-type $La_{0.3}Sr_{0.7}Fe(M')O_{3-\delta}$ (M' = Ga, Al). The calculations suggest that the configurations of A-site and trivalent B-site cations have no essential effect on the chemical potentials of electron holes and oxygen vacancies, the coexistence of which in neighboring sites is, however, unlikely due to coulombic repulsion. For electrons formed due to iron disproportionation under oxidizing conditions, the most stable configuration is in the form of pair clusters with oxygen vacancies. A thermodynamic model taking the repulsion between positively charged defects into account was developed on the basis of lattice simulation results. The model provides adequate description of the experimental $p(O_2)$-T-δ diagrams of $La_{0.3}Sr_{0.7}Fe(M')O_{3-\delta}$, determined by the coulometric titration technique at 923–1223 K in the oxygen partial pressure range from 1×10^{-5} to 0.5 atm. The thermodynamic functions governing the oxygen intercalation process are independent of the defect concentration. The results show that doping with Al^{3+} and Ga^{3+} substantially affects the behavior of iron cations, increasing the tendencies to disproportionation and hole localization, probably due to decreasing covalency of the Fe–O bonds. The latter tendency is more pronounced for aluminum-substituted ferrites, although the total concentrations of point defects in Al- and Ga-containing phases with similar dopant content are quite similar.

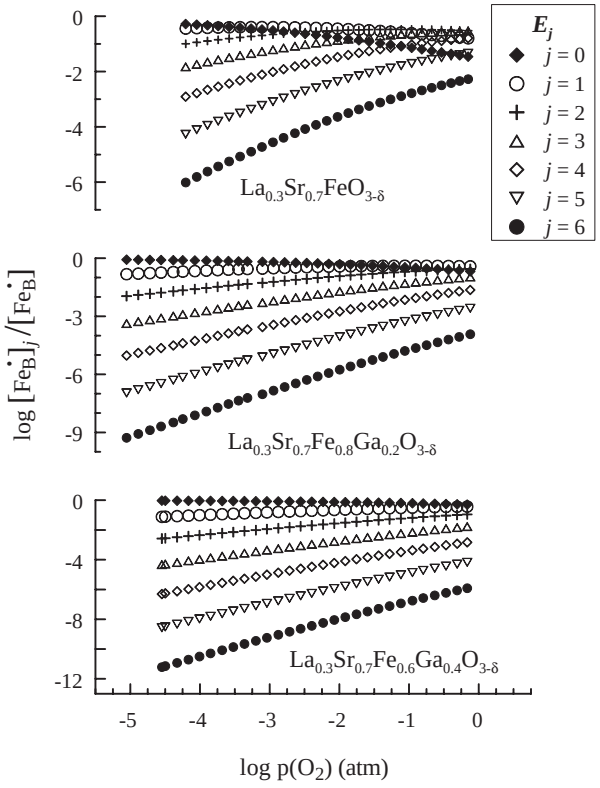

Fig. 15. Hole distribution between the energy levels as function of the oxygen partial pressure and gallium content in $La_{0.3}Sr_{0.7}Fe_{1-x}Ga_xO_{3-\delta}$ at 1073 K.

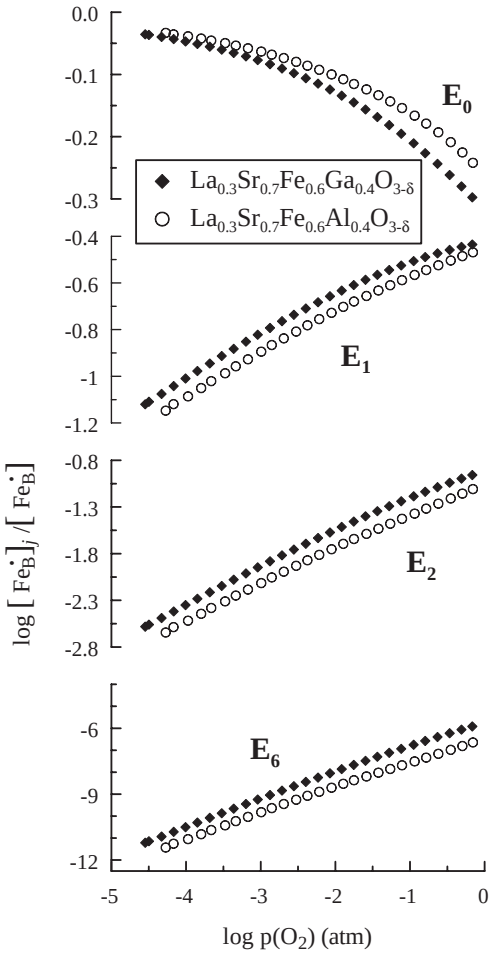

Fig. 16. Comparison of the hole concentration on E_0, E_2 and E_6 levels in Ga- and Al-substituted ferrites at 1073 K.

Acknowledgements

This work was partially supported by the FCT, Portugal (project POCI/CTM/58570/2004 and BPD/11606/2002), the NATO Science for Peace program (project 978002), and the European Science Foundation (OSSEP program). The authors are sincerely grateful to Prof. J.D. Gale for providing the GULP code.

References

[1] H.J.M. Bouwmeester, A.J. Burgraaf, in: A.J. Burgraaf, L. Cot (Eds.), Fundamentals of Inorganic Membrane Science and Technology, Elsevier, Amsterdam, 1996, p. 435.

[2] J. Mizusaki, Solid State Ionics 52 (1992) 79.
[3] T.J. Mazanec, in: H.U. Anderson, A.C. Khandkar, M. Liu (Eds.), Ceramic Membranes I, The Electrochemical Society, Pennington, NJ, 1997, p. 16, PV95-24.
[4] H. Ullmann, N. Trofimenko, F. Tietz, D. Stover, A. Ahmad-Khanlou, Solid State Ionics 138 (2000) 79.
[5] T. Ramos, A. Atkinson, Solid State Ionics 170 (2004) 275.
[6] T.J. Mazanec, T.L. Cable, J.G. Frye and W.R. Kliewer, US Patent 5591315 (1997).
[7] M. Schwartz, J.H. White, A.F. Sammells, US Patent 6214757 (2001).
[8] M.V. Patrakeev, J.A. Bahteeva, E.B. Mitberg, I.A. Leonidov, V.L. Kozhevnikov, K.R. Poeppelmeier, J. Solid State Chem. 172 (2003) 219.
[9] A. Holt, T. Norby, R. Glenne, Ionics 5 (1999) 434.
[10] V.V. Kharton, A.V. Kovalevsky, E.V. Tsipis, A.P. Viskup, E.N. Naumovich, J.R. Jurado, J.R. Frade, J. Solid State Electrochem. 7 (2002) 30.
[11] V.V. Kharton, A.A. Yaremchenko, A.P. Viskup, M.V. Patrakeev, I.A. Leonidov, V.L. Kozhevnikov, F.M. Figueiredo, A.L. Shaulo, E.N. Naumovich, F.M.B. Marques, J. Electrochem. Soc. 149 (2002) E125.
[12] A.A. Yaremchenko, M.V. Patrakeev, V.V. Kharton, F.M.B. Marques, I.A. Leonidov, V.L. Kozhevnikov, Solid State Sci. 6 (2004) 357.
[13] J. Mizusaki, M. Yashihiro, S. Yamauchi, K. Fueki, J. Solid State Chem. 67 (1987) 1.
[14] F.W. Poulsen, Solid State Ionics 129 (2000) 145.
[15] A.N. Petrov, A.Yu. Zuev, I.L.Tikhonova, V.I. Voronin, Solid State Ionics 129 (2000) 179.
[16] F. Boroomand, E. Wessel, H. Bausinger, K. Hilpert, Solid State Ionics 129 (2000) 251.
[17] M.H.R. Lankhorst, PhD Thesis, University of Twente, Enschede, 1997.
[18] M.V. Patrakeev, E.B. Mitberg, A.A. Lakhtin, I.A. Leonidov, V.L. Kozhevnikov, V.V. Kharton, M. Avdeev, F.M.B. Marques, J. Solid State Chem. 167 (2002) 203.
[19] M.V. Patrakeev, E.B. Mitberg, A.A. Lakhtin, I.A. Leonidov, V.L. Kozhevnikov, K.R. Poeppelmeier, Ionics 4 (1998) 191.
[20] F.W. Poulsen, G. Lauvstad, R. Tunold, Solid State Ionics 72 (1994) 47.
[21] V.V. Kharton, A.L. Shaulo, A.P. Viskup, M. Yu. Avdeev, A.A. Yaremchenko, M.V. Patrakeev, A.I. Kurbakov, E.N. Naumovich, F.M.B. Marques, Solid State Ionics 150 (2002) 229.
[22] V.V. Kharton, A.A. Yaremchenko, M.V. Patrakeev, E.N. Naumovich, F.M.B. Marques, J. Eur. Ceram. Soc. 23 (2003) 1417.
[23] K. Yamaji, T. Horita, M. Ishikawa, N. Sakai, H. Yokokawa, Solid State Ionics 121 (1999) 217.
[24] J.D. Gale, J. Chem. Soc., Faraday Trans. 93 (1997) 629.
[25] J.D. Gale, A.L. Rohl, Mol. Simul. 29 (2003) 291.
[26] M.S. Islam, J. Mater. Chem. 10 (2000) 1027.
[27] M.S. Islam, Solid State Ionics 154–155 (2002) 75.
[28] M.R. Levy, B.C.H. Steel, R.W. Grimes, Solid State Ionics 175 (2004) 349.
[29] M.H.R. Lankhorst, H.J.M. Bouwmeester, H. Verweij, J. Am. Ceram. Soc. 80 (1997) 2175.
[30] V.N. Chebotin, Physical Chemistry of Solids, Khimiya, Moscow, 1982.
[31] IUPAC, Commission on Thermodynamics; Oxygen, International Thermodynamic Tables of the Fluid State-9, Blackwell Scientific Publications, Oxford, 1987.
[32] S. Ling, Phys. Rev., B 49 (1994) 864.
[33] S. Ling, Solid State Ionics 70–71 (1994) 686.
[34] S. Ling, J. Phys. Chem. Solids 55 (1994) 1445.
[35] M.S. Khan, M.S. Islam, D.R. Bates, J. Phys. Chem., B 102 (1998) 3099.
[36] G.W. Lewis, C.R.A. Catlow, J. Phys. C. Solid State Phys. 18 (1985) 1149.
[37] M. Cherry, M.S. Islam, C.R.A. Catlow, J. Solid State Chem. 118 (1995) 125.
[38] M.V. Patrakeev, I.A. Leonidov, V.L. Kozhevnikov, V.V. Kharton, Solid State Sci. 6 (2004) 907.
[39] V.N. Tikhonovich, O.M. Zharkovskaya, E.N. Naumovich, I.A. Bashmakov, V.V. Kharton, A.A. Vecher, Solid State Ionics 160 (2003) 259.